

## Hydroacoustic forcing function modeling using DNS database

By I. Zawadzki<sup>1</sup>, J. L. Gershfeld<sup>1</sup>, Y. Na<sup>2</sup> AND M. Wang<sup>3</sup>

A wall pressure frequency spectrum model (Blake 1971) has been evaluated using databases from direct numerical simulations (DNS) of a turbulent boundary layer (Na & Moin 1996). Good agreement is found for moderate to strong adverse pressure gradient flows in the absence of separation. In the separated flow region, the model underpredicts the directly calculated spectra by an order of magnitude. The discrepancy is attributed to the violation of the model assumptions in that part of the flow domain. DNS computed coherence length scales and the normalized wall pressure cross-spectra are compared with experimental data. The DNS results are consistent with experimental observations.

---

### 1. Introduction

Understanding the physics of the interaction of the airfoil turbulent boundary layers incident to the trailing edge is of interest to the designers of practical airframe components and lifting surfaces. Flow at trailing edges involves complex phenomena including adverse pressure gradient effects, flow separation, vortex shedding, and pressure scattering at the edge boundary discontinuity. It is not surprising then, that even an approximate treatment of practical cases, particularly from the vantage point of sound generation, encounters serious difficulties. Inviscid flow theories that capture the purely acoustic interaction of the flow with the trailing edge have been developed (Howe 1978, 1988). Several experiments have also been performed (Brooks & Hodgson 1981, Blake 1986) which shed some light on the physics of the viscous flow problem. Well designed experimental efforts are invaluable in improving our understanding of the phenomena as demonstrated by Gershfeld *et al.* (1988) and Blake & Gershfeld (1989). They are, however, limited in terms of providing global information about the flow. One of the principal weaknesses of the experimental estimations of the flow acoustic source terms is that they are essentially ad hoc. The experimentalist must assume *a priori* which of the several potential flow acoustic sources are relevant so that estimates of the dipole source strength may be made. It is only when the direct dipole sound field is measured that the empirical estimates of the forces associated with the direct dipoles can be determined to be relevant. Unfortunately, there have been very few successful measurements of the trailing edge direct dipole sound field. When the inviscid

1 David Taylor Model Basin, NSWC/CD

2 University of Illinois at Urbana Champaign

3 Center for Turbulence Research

turbulent flow dipole sound formulations of Howe (1978, 1988) are applied with a Kutta condition, the predicted dipole sound field does not agree with experimental data (Brooks & Hodgson 1981). Only when the Kutta condition is removed does his model agree. Viscous DNS calculations may add insight into this modeling dilemma. The advantage of flow databases obtained by means of numerical simulations is that they contain spatial and temporal data throughout the flow domain which is not attainable in laboratory experiments.

Trailing edge flows of interest often include both attached and separated flow regimes (Brooks & Hodgson 1981, Blake 1984). With that in mind, we utilize the numerical database developed by Na & Moin (1996). Since the database includes flow with adverse pressure gradient and separation, it was well suited as a first step towards modeling of the more complex flow – trailing edge interactions. Our goals were two-fold. First, we wanted to re-examine the database from the point of view of an aeroacoustician to complement the results already presented by Na & Moin. (There is a certain degree of skepticism among the applied community as to whether relatively low Reynolds number DNS calculations can be of use for predicting high Reynolds number flows found in practical realizations. Wall pressure spectra reported by Na & Moin show many features and trends observed in the experiments, a hint that DNS calculations are, in fact, relevant.) Our second goal was to revisit a wall pressure model developed long before there were means of reliably assessing its accuracy or limits of applicability. DNS database provides such means since it contains both the complete flow data necessary for the input to the model as well as directly calculated wall pressures which can be used to verify or invalidate the model predictions.

## 2. Wall pressure model

In the following sections  $x$ ,  $y$ , and  $z$  (or  $x_i$ ,  $i = 1, 2, 3$ ) will denote the streamwise, wall-normal, and spanwise coordinate, respectively, while  $u$ ,  $v$ ,  $w$  (or  $u_i$ ,  $i = 1, 2, 3$ ) will be the corresponding fluctuating velocity components. Other quantities pertaining to a given coordinate direction will carry an appropriate coordinate subscript (e.g.  $k_x$  is the streamwise component of the wave-number vector  $\mathbf{k}$ ). For an incompressible flow invoking the usual boundary layer approximation, evaluation of pressure can be reduced to solving the Poisson's equation (see, for example, Blake 1986)

$$\nabla^2 p(\mathbf{x}, t) = -2\rho_0 \frac{\partial v}{\partial x} \frac{\partial U(\mathbf{x}, t)}{\partial y} - \rho_0 \frac{\partial^2 u_i u_j}{\partial x_i \partial x_j} \quad (1)$$

where  $U$  is the mean streamwise velocity. Lilley (1960) derived a solution of Eq. (1) in terms of the wave number frequency spectrum of the wall pressure,

$$\Phi_{pp}(\mathbf{k}, \omega) = \frac{4\rho_0^2 k_x^2}{k_x^2 + k_z^2} \int_0^\infty dy \int_0^\infty dy' e^{-(y+y')\sqrt{k_x^2+k_z^2}} \tau(y)\tau(y')\Phi_v(y, y'; \mathbf{k}, \omega), \quad (2)$$

where  $\mathbf{k} = (k_x, k_z)$  is the wave number vector in the plane parallel to the wall,  $\tau(y) = \frac{\partial U}{\partial y}$  is the mean shear, and  $\Phi_v(y, y'; \mathbf{k}, \omega)$  is the cross-spectral density of

the vertical velocity field. Equation (2) was derived under the assumption that the second term on the right hand side of Eq. (1) is negligible compared with the first term, and that the source field is spatially homogeneous in the  $(k_x, k_z)$  plane. Blake (1971) further modified Lilley's solution by introducing a separable model for the vertical velocity spectrum:

$$\Phi_v(y, y'; \mathbf{k}, \omega) = \overline{v^2}(y) \hat{R}_{vv}(y, y') \phi_{vv}^x(k_x) \phi_{vv}^z(k_z) \phi_m(\omega - k_x U_c). \quad (3)$$

Here,  $\overline{v^2}(y)$  is the mean square of vertical fluctuating velocity,  $\hat{R}_{vv}(y, y')$  is a normalized correlation in the  $y$ -direction,  $\phi_m(\omega - k_x U_c)$  is the moving axis spectrum,  $U_c$  is the convection velocity, and  $\phi_{vv}^x(k_x)$  and  $\phi_{vv}^z(k_z)$  are wave number spectra defined as the Fourier transforms of, respectively, normalized streamwise and spanwise separation correlation functions of vertical velocity. (We use the lowercase symbol  $\phi$  to denote the normalized spectrum functions. The normalization is:  $\int_{-\infty}^{\infty} \phi(k_i) dk_i = 1$ .)

Using (3) Blake (1971) obtains the wall pressure frequency spectrum by integrating Eq. (2) with respect to the wave number components  $k_x$ ,  $k_z$ . The final result can be written in the form

$$\Phi_{pp}(\omega) = 4\rho_0^2 \int_0^\infty dy \int_0^\infty dy' \overline{v^2}(y) \hat{R}_{vv}(y, y') \tau(y) \tau(y') \frac{1}{U_C} \phi_{vv}^x\left(\frac{\omega}{U_C}\right) I\left(\frac{\omega}{U_C}, y, y'\right), \quad (4)$$

where

$$I(k_x, y, y') = \int_{-\infty}^{\infty} dk_z \frac{k_x^2}{k_x^2 + k_z^2} e^{-(y+y')\sqrt{k_x^2+k_z^2}} \phi_{vv}^z(k_z). \quad (4a)$$

Taylor's hypothesis of frozen convection was used in the integration leading to Eq. (4). Mathematically, the hypothesis states that  $\phi_m(k_x - \frac{\omega}{U_c}) = \delta(k_x - \frac{\omega}{U_c})$ , which leads to the following equivalence of the normalized wave number spectrum  $\phi_{vv}^x(k_x)$  and the frequency spectrum  $\phi_{vv}(\omega)$ :

$$\phi_{vv}^x(k_x) = \frac{1}{U_c} \phi_{vv}\left(\frac{\omega}{U_C}\right). \quad (5)$$

In order to evaluate Eq. (4,4a) one needs to compute the vertical correlation  $\overline{v^2}(y) \hat{R}_{vv}(y, y')$ , the mean shear  $\tau(y)$ , and the wave number spectra  $\phi_{vv}^x(k_x)$  and  $\phi_{vv}^z(k_z)$  (See discussion in sections 4.2 and 4.3 on selecting the location at which the spectra should be evaluated). Calculation of these quantities from the DNS database is a straightforward matter. We should point out that in principle one could compute the cross-spectral density function  $\Phi_v(y, y'; \mathbf{k}, \omega)$  without resorting to the separable model (Eq. (3)) and integrate numerically Eq. (2) directly to obtain the pressure frequency spectrum. Besides not being physically revealing, such a procedure, however, would be prohibitively expensive in terms of computational time and memory.

We should also point out the modeling described above is applicable only to convective wave numbers near  $k_x = \omega/U_C$ . In other words, Eq. (4) does not encompass sources outside of the convective range. Other models of wall pressure

spectrum (Chase 1980) could be used to include broader range of wave numbers. However, trailing edge noise is dominated by scattering of convective wall pressures (with boundary discontinuity providing the conversion mechanism to acoustic wave numbers - Howe (1979)). Therefore, from the standpoint of acoustic radiation, Blake's simplified approach to computing the wall pressure spectrum should be sufficient.

### 3. DNS database

Most of the data presented here (with the exception of Fig. 2a) will refer to the separated flow calculation in the Na & Moin (1996) database. Following Na & Moin, we introduce the non-dimensional variables given by

$$u_i^* = \frac{u_i}{U_0}, \quad x_i^* = \frac{x_i}{\delta_{in}^*}, \quad t^* = \frac{tU_0}{\delta_{in}^*}, \quad p^* = \frac{p}{\rho U_0^2} \quad (6)$$

where  $U_0$  is the mean velocity at inlet and  $\delta_{in}^*$  is the (dimensional) inlet displacement thickness. All quantities discussed in the following sections, including the wave number and frequency spectra, incorporate this nondimensionalization. The superscript \*, denoting non-dimensional quantities, has been dropped to simplify notation.

In order to establish for the reader the reference coordinates for different flow regimes, the mean streamlines were reproduced in Fig. 1.

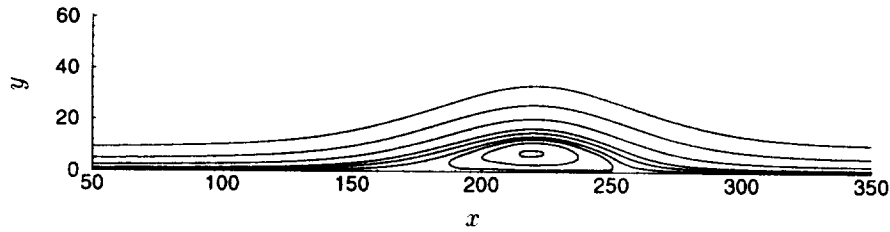


FIGURE 1. Mean flow streamlines.

In non-dimensional units (Eq. 6) the streamwise and spanwise extent of the computational domain is, respectively, 350 and 50. The vertical height is 64. Flow separation is induced by prescribing suction-blowing velocity profile along the upper boundary. As a result, strong adverse pressure gradient exists between the non-dimensional coordinates  $x = 90$  and  $x = 150$ . Boundary layer separation occurs around  $x = 160$ . Coordinate  $x = 220$  corresponds to the center of the separation bubble. Grid resolution is  $513 \times 193 \times 129$  points in the streamwise, wall-normal, and spanwise directions, respectively. The Reynolds number based on inlet momentum thickness and free-stream inlet velocity is 300. For additional details of the flow calculations, including description of the computational method, we refer the reader to Na & Moin (1996).

## 4. Results and discussion

### 4.1 Wall pressure data analysis

Standard tools of correlation analysis were utilized to analyze the DNS calculated wall pressure data. We wanted to establish whether DNS results, which are obtained for a relatively low Reynolds number, are in agreement with experimental data. The comparisons also served to validate our numerous computer codes. Let  $\mathbf{r} = (r_x, r_z)$  be a separation vector in a plane parallel to the wall. Defining the cross-correlation function of a field quantity  $q$  as an ensemble average,

$$R_{qq}(\mathbf{x}, \mathbf{r}, \tau) = \langle q'(\mathbf{x}, t)q'(\mathbf{x} + \mathbf{r}, t + \tau) \rangle, \quad (7)$$

the cross spectrum function is the Fourier transform of (7) with respect to the time delay:

$$\Phi_{qq}(\mathbf{x}, \mathbf{r}, \omega) = \int_{-\infty}^{\infty} R_{qq}(\mathbf{x}, \mathbf{r}, \tau) e^{-i\omega\tau} d\tau. \quad (8)$$

Coherence is defined as the cross spectrum squared, normalized by the local autospectrum:

$$\gamma^2(\mathbf{x}, \mathbf{r}, \omega) = \frac{|\Phi_{qq}(\mathbf{x}, \mathbf{r}, \omega)|^2}{|\Phi_{qq}(\mathbf{x}, 0, \omega)||\Phi_{qq}(\mathbf{x} + \mathbf{r}, 0, \omega)|}. \quad (9)$$

The Corcos (1963) model of the cross-spectrum of the wall pressure,  $p$ , has the form

$$\Phi_{pp}(r_x, r_z, \omega) = \Phi(\omega) A\left(\frac{\omega r_x}{U_C}\right) e^{-i\frac{\omega r_x}{U_C}} B\left(\frac{\omega r_z}{U_C}\right), \quad (10)$$

with  $A$  and  $B$  modeled as exponentially decaying functions. These functions are calculated by expressing the square root of the coherence (Eq. 9) in terms of the similarity variable  $\omega r/U_C$ . The results for the streamwise component are shown in Fig. 2.

As a reference, the results for the zero pressure gradient flow, obtained using a separate DNS database (Na & Moin 1996, Chapter 3), are plotted in Fig. 2a. They are closely described by the experimentally observed exponential function with decay constant  $a = -0.125$  (Brooks & Hodgson 1981). Abraham & Keith (1995) report similar agreement with the experimental results for DNS simulated turbulent channel flow. When an adverse pressure gradient is present, however, the streamwise coherence curves decay at a much faster rate (Fig. 2b) and the Corcos constant has to be altered. A reasonable fit is obtained with a decay constant  $a = 0.4$ . This trend is in agreement with the observations of Schloemer (1967). We evaluated the Corcos "A" function for several streamwise locations corresponding to varying degree of pressure gradient and found that the decay constant increases monotonically with the pressure gradient.

By contrast, we found the rate of decrease for the spanwise Corcos similarity function "B" to be practically independent of the pressure gradient. As shown in Fig. 3a, the results at  $x = 120$  agree reasonably with the experimentally observed exponential rate of decrease  $b = -0.7$ . The situation changes dramatically, however,

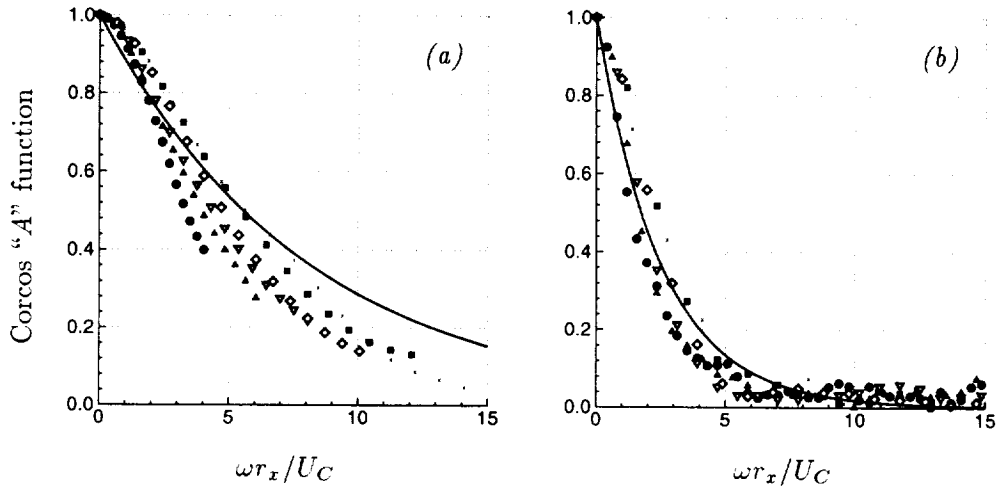


FIGURE 2. Streamwise coherence in Corcos similarity form. (a) Zero pressure gradient flow for selected values of frequency  $\omega$ :  $\bullet$  0.31,  $\blacktriangle$  0.47,  $\nabla$  0.63,  $\diamond$  0.79,  $\blacksquare$  0.94,  $\times$  1.1; —  $e^{-0.125\omega r_x / U_C}$ . (b) Adverse pressure gradient flow at  $x = 120$ ;  $\omega$  =  $\bullet$  0.21,  $\blacktriangle$  0.31,  $\nabla$  0.42,  $\diamond$  0.52,  $\blacksquare$  0.63,  $\times$  0.73; —  $e^{-0.4\omega r_x / U_C}$ .

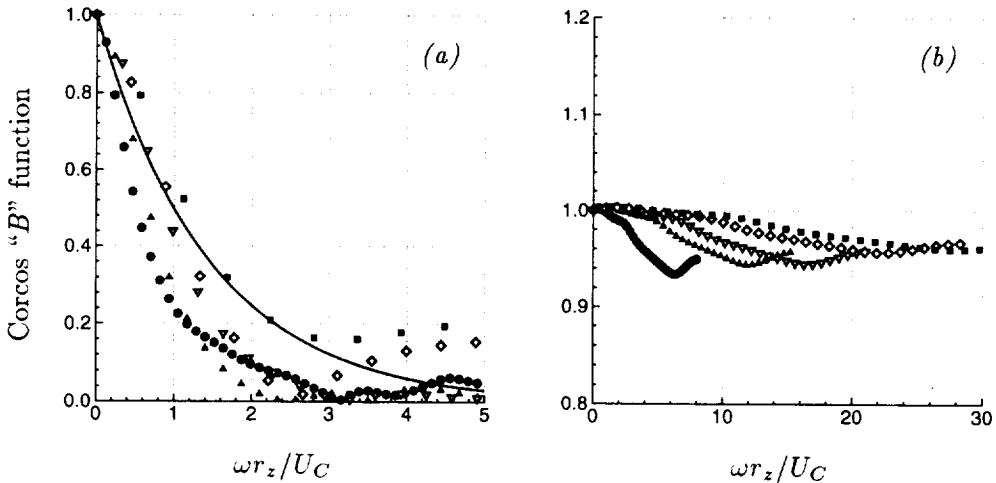


FIGURE 3. Spanwise coherence in Corcos similarity form. (a)  $x = 120$ , (b)  $x = 220$ ; for selected values of frequency:  $\bullet$  0.21,  $\blacktriangle$  0.42,  $\nabla$  0.59,  $\diamond$  0.8,  $\blacksquare$  1.0; —  $e^{-0.7\omega r_x / U_C}$ .

when the function is evaluated inside the separation bubble (Fig. 3b). All the curves stay very close to a constant value of unity which demonstrates that the wall pressure in the separated flow region is essentially two-dimensional.

Another experimentally measurable characteristic of the wall pressure is given by the frequency dependent streamwise and spanwise length scales. These are obtained by calculating the coherence for a suitably chosen separation vector and integrating

the result over the separation distance. For example, the spanwise length scale is given by:

$$\Lambda_z(\mathbf{x}, \omega) = \int_0^\infty \sqrt{\gamma^2(\mathbf{x}, r_z, \omega)} dr_z \quad (11)$$

where  $r_z$  is the spanwise separation distance. Gershfeld *et al.* (1988) have calculated both spanwise and streamwise coherence length scales for their trailing edge measurements which included adverse pressure gradient effects. They have assumed the Corcos relation:  $\Lambda = C \frac{U}{\omega}$  and proceeded to calculate the proportionality constant  $C$  for varying flow conditions. They have found the constant value to range between 0.5 and 1.5 for the spanwise length scales and between 1.75 and 6.0 for the streamwise length scales. Figure 4 shows that the DNS calculated length scales fall within the range observed by Gershfeld *et al.*

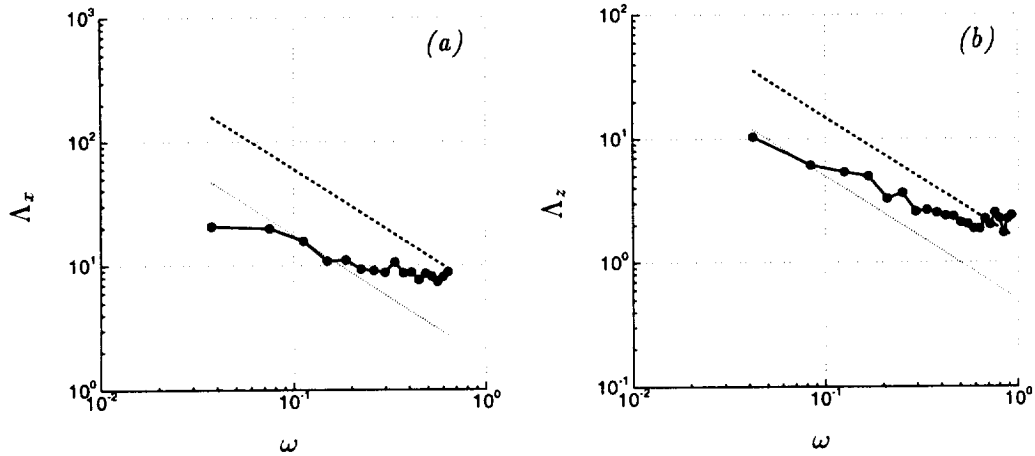


FIGURE 4. (a) Streamwise coherence length scales: • DNS, .....  $1.75U/\omega$ , ---  $6.0U/\omega$ . (b) Spanwise coherence length scales: • DNS, .....  $1.5U/\omega$ , ---  $0.5U/\omega$ .

One of the quantities required for the integrand of Eq. (4) is the two-point correlation of vertical velocity. Hunt *et al.* (1987) have demonstrated that for boundary layer flows the normalized correlation has an approximately self-similar form when expressed as a function of  $y/y'$ , ( $0 \leq y \leq y'$ ). In Fig. 5 we plot the correlation with the normalization as prescribed by Hunt *et al.*

In the attached region (Fig. 5a) the self-similarity can be clearly observed for values of  $y'$  up to 4. At the streamwise location where the correlation in Fig. 5a was calculated ( $x = 80$ ), the  $y' = 8$  position lies too close to the boundary layer edge so the self-similarity is not expected to be preserved there. On the other hand, at the center of the separation bubble the boundary layer thickness is much larger than 8, and as a result none of the curves plotted in Fig. 5b shows drastic departure from the other curves. However, the collapse is not as good as for the first four  $y$ -locations in Fig. 5a. This is not surprising as the flow in the separated region does not at all resemble a typical boundary layer profile.

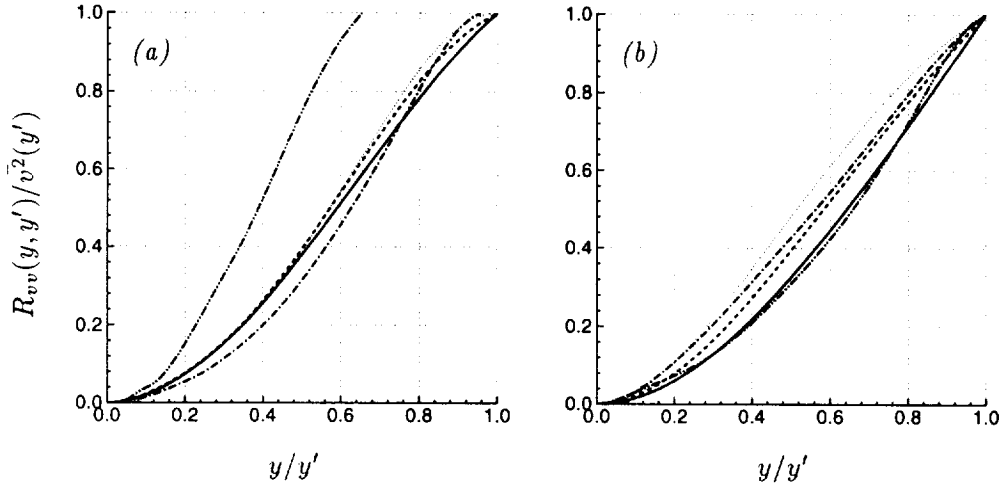


FIGURE 5. Two-point correlation of wall-normal velocity component, (a)  $x = 80$ , (b)  $x = 220$ ; —  $y' = 0.5$ , - - -  $y' = 1.0$ , ·····  $y' = 2.0$ , - · -  $y' = 4.0$ , - · - · -  $y' = 8.0$ .

#### *4.2 Discussion of the wall pressure model assumptions*

For the sake of completeness we list the assumptions made in deriving the wall pressure model Eq. (4):

- 1 . Boundary layer approximation.
- 2 . Spatial homogeneity of the source term in the planes parallel to the wall.
- 3 . Dominance of the linear source term over the nonlinear part.
- 4 . Spatial localization (in the wall-normal direction) of the sources.
- 5 . Spectral separability of the source field.
- 6 . Taylor's hypothesis of frozen convection.

Assumption 1 is readily satisfied before the flow separation. This allows neglecting certain terms when deriving the Eq. (1). In the separated region, instantaneous velocity vector plots (Na & Moin 1996, Fig 5.14) show very small velocity vectors with frequent flow reversal in the region between the wall and the separated shear layer. Therefore, in this region the boundary layer approximation, which presumes preferable mean flow direction with the streamwise component being much larger than the other components, is no longer valid.

Assumption of spatial homogeneity is implicit in expressing the pressure and velocity fields in terms of wave number spectra (Eqs. (2) and (3)). Strictly speaking one cannot expect to find homogeneity in the streamwise direction in a spatially developing flow. All we can hope for is for the flow to be “locally homogeneous”, in the sense that the streamwise variation is locally small enough so that computing the ensemble average (Eq. 7) and taking the Fourier transform with respect to the streamwise separation is physically meaningful at least for a certain range of the wave numbers. Figure 6 shows one of the diagnostics of the spatial homogeneity. It shows two-point streamwise separation correlation contours of the wall pressure. One can see that up to the point of separation ( $x < 150$ ) and inside the separated

region ( $190 < x < 260$ ), the field is nearly homogeneous (contour lines are nearly parallel to the abscissa). In the vicinity of the separation point, ( $150 < x < 190$ ) the correlation function is strongly dependent on the streamwise location.

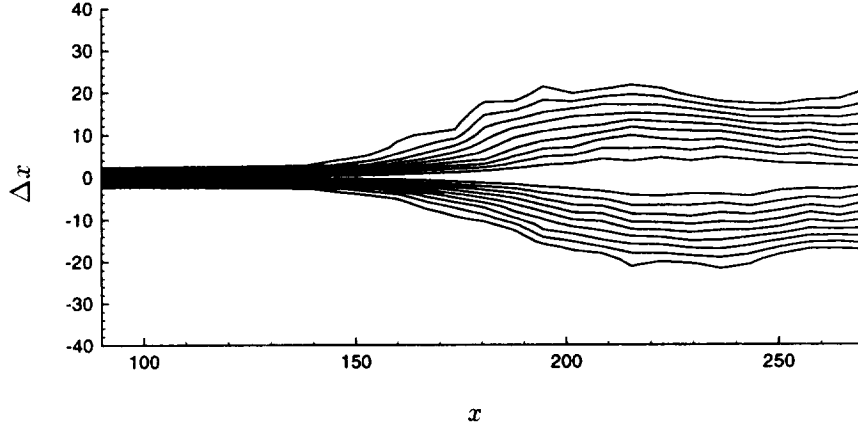


FIGURE 6. Wall pressure two-point streamwise separation correlation contours.

The next approximation – neglecting the nonlinear term in Eq. (1) – used to be considered very plausible until the work of Kim (1989). Kim has demonstrated that the contributions of both terms to the wall pressure are of comparable magnitude, with the total pressure exceeding both the linear component's contribution by about 30 percent. Therefore, we expect Eq. (2) to underestimate the spectral levels of the wall pressure.

Spatial localization of the sources is the key to representing the vertical velocity spectrum via Eq. (3), which de-facto puts all the dependence on the  $y$ -coordinate in the correlation term and makes the remaining terms independent of  $y$ . We plotted the magnitude of the  $y$ -coordinate dependent part of the source term in Fig. 7.

One can see a clearly pronounced peak very close to the wall for locations upstream of the separation bubble (Fig. 7a). At the detachment point (Fig. 7b,  $x = 160$ ), the height of the peak has decreased by an order of magnitude and its effective width has become comparable with the thickness of the boundary layer. In the center of the separated region ( $x = 220$ ), the maximum of the source term has moved away from the wall to coincide with the location of the shear layer and the peak has become even broader. In the reattachment region ( $x = 280$ ), a new maximum begins to reappear near the wall.

The assumption of spectral separability states that the wave number spectrum in the plane parallel to the wall can be expressed as a product of two functions, each dependent on, respectively, only the streamwise and spanwise wave number component. It is a convenient tool which allows obtaining the final result (Eq. (4)) in a simple form. In principle, one could compute the exact two-dimensional spectrum by calculating two-point correlation for all possible pairs of streamwise and spanwise separations and taking two-dimensional Fourier transform of the result.

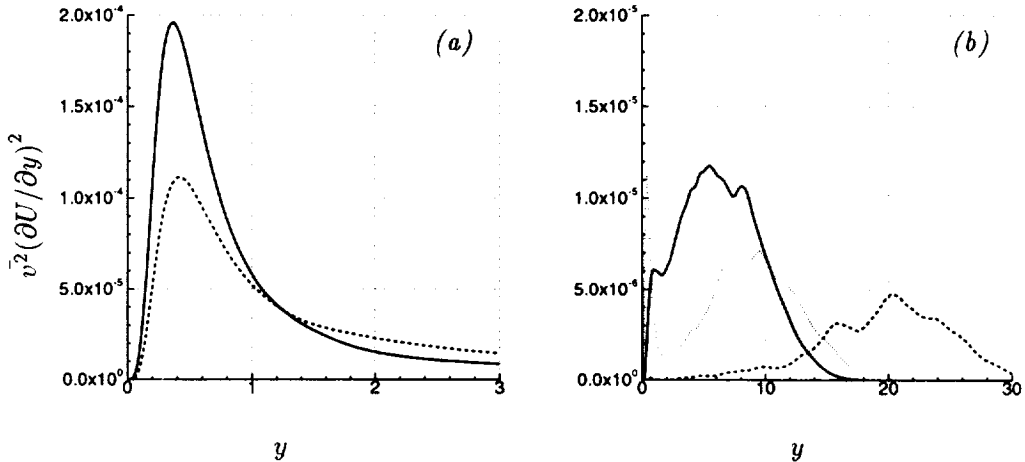


FIGURE 7. Wall pressure model source term as a function of the distance from the wall, (a): —  $x = 80$ , - - -  $x = 120$ , (b): —  $x = 160$ , - - -  $x = 220$ , .....  $x = 280$ .

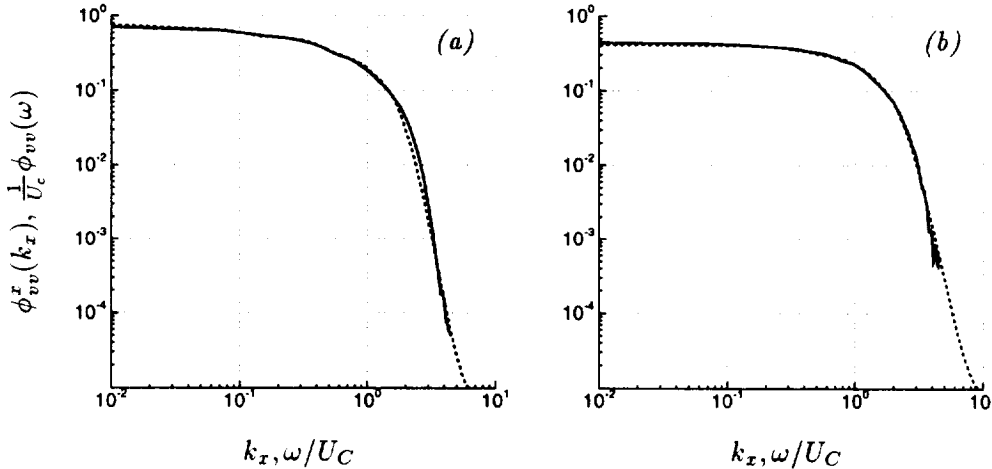


FIGURE 8. Normalized spectra of vertical velocity component at (a)  $(x, y) = (80, 0.76)$ , (b)  $(x, y) = (130, 0.76)$ ; ——  $\phi_{vv}^x(k_x)$ , - - -  $\frac{1}{U_c} \phi_{vv}(\omega)$ .

We have not performed such calculations and, therefore, cannot comment on the errors incurred by using the separable representation.

The last approximation, the Taylor's hypothesis of frozen convection, can be tested by calculating and comparing the spectra in Eq. (5). Before making the comparison, one must choose a proper value for the convection velocity  $U_C$ . A natural choice is the local mean velocity. The normalized spectra calculated in the  $y = 0.76$  plane at two selected streamwise locations,  $x = 80$  and  $x = 130$ , are shown in Fig. 8a,8b. The local mean velocity  $U_{local}$  at these coordinates is, respectively,

0.56 and 0.29. Clearly, with this choice of  $U_C = U_{local}$ , the spectra agree very well even when evaluated at the location with a severe local adverse pressure gradient (Fig. 8b).

#### 4.3 Comparison of model predictions with DNS data

The model predictions are calculated by numerically integrating (4). The integration is straightforward once all the ingredients of the integrand are known. There are, however, issues concerning the determination of the convection velocity  $U_C$  and the wavenumber spectra  $\Phi_{vv}^x(k_x)$  and  $\Phi_{vv}^z(k_z)$  in the integrand, which deserve a brief discussion.

Using the wall pressure convection velocity inferred from time-space correlations calculated by Na & Moin would not be compatible with the spirit of this work. One would prefer to rely exclusively on the velocity field data and not to use any variable that is a characteristic of the quantity that we are trying to predict. With regard to the normalized velocity wavenumber spectra, one expects them to be independent of  $y$ , since the  $y$ -dependence has been included in the vertical correlation function in the separable representation (3). Under this premise it appears reasonable to pick a single constant- $y$  plane and take the  $\Phi_{vv}^x(k_x)$  and  $\Phi_{vv}^z(k_z)$  there as the representative wavenumber spectra required in (4). The convective velocity  $U_C$  can be approximated by the local mean velocity, as demonstrated by Fig. 8. Ideally, one would prefer the selected  $y$ -plane to coincide with the location of maximum source magnitude, as the contribution from the vicinity of the source peak is expected to dominate over contributions from all other locations (Blake 1984). (Of course, the notion that the maximum source magnitude contributes most to the wall pressure is valid only when the shear layer is close enough to the wall. Otherwise, the effects of the exponential factor in Eq. (4a) may become significant). However, the difference should be small even if the selected plane deviates from the source peak, so long as it lies within the active source region where the separable representation (3) holds.

In the present calculations, the vertical-velocity wavenumber spectra are approximated by those at  $y \approx 0.76$  for the streamwise stations  $x = 80$  and  $120$ ,  $y = 7.07$  for  $x = 160$ , and  $y = 19.67$  for  $x = 220$ . Our choices of the  $y$ -planes are limited by the available DNS data (there are only five  $y$ -planes with complete space-time velocity information saved in the original DNS database). The  $U_C$  value is approximated by the local mean velocity at the given  $(x, y)$ -position.

The model predictions at four different streamwise locations, representing different flow regimes, are shown in Figs. 9 and 10. The directly computed pressure spectra are also plotted for comparison. In the attached flow region at  $x = 80$  (Fig. 9a) and  $x = 120$  (Fig. 9b), the agreement between model and DNS is very good. The under-prediction at low frequencies may be attributed to neglecting the non-linear terms in Eq. (1). Considering that the contributions from the retained and neglected term are of comparable magnitude (Kim 1989), and given the approximations involved in the evaluation of the integrand, a discrepancy (underestimate) should be expected.

At the flow separation point  $x = 160$  (Fig. 10a) familiar underprediction at low frequencies is again observed. There is also a marked difference at the high end of

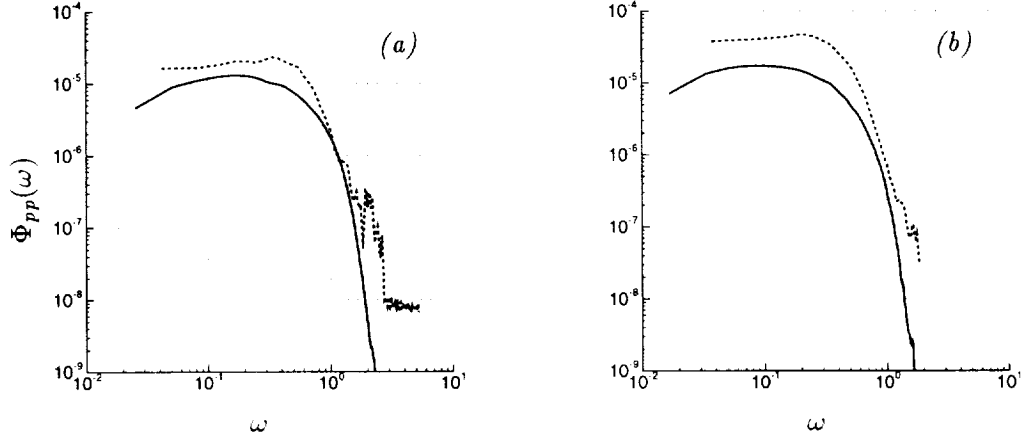


FIGURE 9. Wall pressure frequency spectrum, (a)  $x = 80$ , (b)  $x = 120$ ; — model (Eq. 4), - - - DNS.

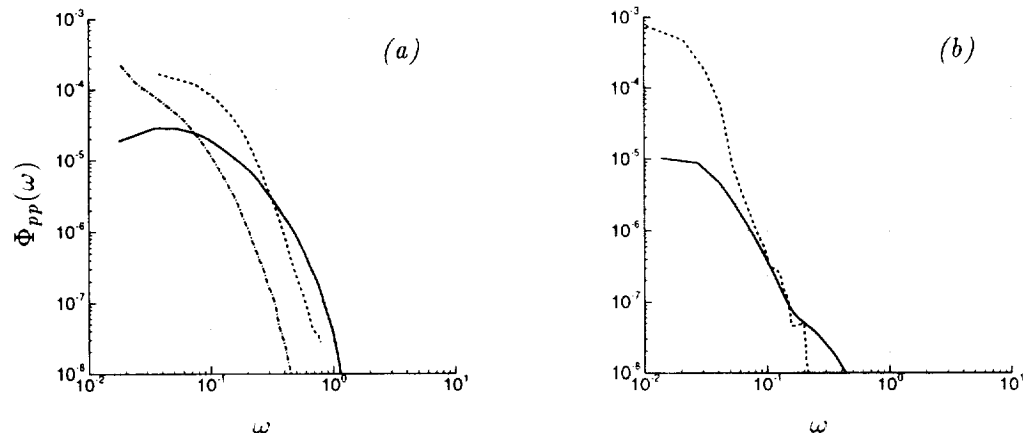


FIGURE 10. Wall pressure frequency spectrum. (a)  $x = 160$ ; — model (Eq. 4 using velocity spectrum at  $y = 7.07$ ), - - - model (Eq. 4 using velocity spectrum at  $y \approx 2.28$ ), - - - DNS. (b)  $x = 220$ ; — model (Eq. 4), - - - DNS.

the frequency spectrum (compare solid and dashed lines in Fig. 10). One possible reason for the "misalignment" of the spectra could be an improper choice (restricted by the limited available data) of the representative wavenumber spectrum  $\Phi_{vv}^x(k_x)$  and the corresponding convection velocity  $U_C$ . Indeed, if we use the  $y \approx 2.28$  plane instead of our first choice  $y = 7.07$ , the model spectrum shifts towards lower frequencies (Fig. 10a). These results seem to confirm that the optimum choice would be  $y \approx 5$ , i.e. near the location of the peak of the source term (cf Fig. 7b).

In the separated region (Fig. 10b), the model and DNS results differ by more than an order of magnitude. As discussed in section 4.2 the model failure may be

attributed to the fact that the nature of the flow in this regime is largely incompatible with the model assumptions. For the model to perform well, the wall pressure has to be the signature of a spectrally separable source localized in the  $y$ -direction (cf. (3)), moving at a constant speed. This condition is violated, given the large vertical extent and the wide range of flow characteristics in the separated zone. The exponential decay of the Green's function (cf Eq. 4a) accentuates the contribution of the eddies closer to the wall than the detached shear layer, particularly in the high frequency range. In other words, less energetic eddies may compete, in terms of their contribution to the wall pressure, with higher intensity sources depending on their relative proximity to the wall. For the separated flow, therefore, a "representative" source  $y$ -layer with a single convective velocity is difficult, if not impossible, to identify.

### 5. Conclusions and future work

There is an ongoing need for an accurate prediction of wall pressure spectrum in aeroacoustic engineering applications. Since current computational capabilities cannot provide the necessary space and time resolution for computing the pressure spectrum directly (for the Reynolds numbers of interest), appropriate models have to be utilized. In this project we have demonstrated that a simplified model developed for a flat plate turbulent boundary layer can be used for predicting wall pressure frequency spectrum of a flow with a strong adverse pressure gradient. In practical cases RANS calculations could provide the mean shear and wall-normal turbulence intensity required by the model. Hunt *et al's.* (1987) similarity model can be used for the correlation function of vertical velocity. The wave number spectra of vertical velocity, also needed as input to the model, can be calculated from experimental two-point correlation flow measurement.

Our results also show that in the separated region the model's performance is unsatisfactory. It is perhaps premature to assume that the model would fail for any separated flow scenario. From the exponential form of the Green's function in Eq. (4a), it is apparent that the contribution of the shear layer as a source term of the wall pressure rapidly diminishes with the distance from the wall. Therefore, the accuracy of the model's prediction should depend on the distance between the shear layer and the wall as well as on the strength of the shear layer relative to the turbulence level in the separation bubble. In any event, the non-linear pressure source terms need to be included in order to obtain accurate wall pressure spectrum predictions for a broad class of separated flows.

We plan to use the experience gained during the course of this work as a stepping stone towards modeling, with the aid of DNS and LES simulations, of wall pressure spectra of more complex trailing edge flows.

### Acknowledgements

The authors are thankful to Dr. W. Blake for his guidance and many enlightening discussions, and to Prof. P. Moin for helpful suggestions during the summer program. Support for this work provided by ONR, with P. Purtell as program manager, is gratefully acknowledged.

## REFERENCES

- ABRAHAM, B. M. AND KEITH, W. K. 1995 Analysis of the wall pressure field from a numerical simulation of turbulent channel flow. ASME NCA-Vol 19/FED-Vol. 230. *Flow Noise Modeling, Measurement and Control.* 55-65.
- BLAKE, W. K. 1971 Turbulent velocity and pressure fields in boundary layer flows over rough surfaces. *Symposium on Turbulence in Liquids*, Univ. of Missouri, Rolla, 114-122.
- BLAKE, W. K. 1984 Trailing edge flow and aerodynamic sound, Part 1 and Part 2, DTNSRC Report - 83/113.
- BLAKE, W. K. 1986 Mechanics of flow-induced sound and vibration I, II Academic Press, London.
- BLAKE, W. K. AND GERSHFELD J. L. 1989 The aeroacoustics of trailing edges. *Ch. 10, Lecture Notes in Engineering*, Springer Verlag. 46, 457-532.
- BROOKS, T. F. AND HODGSON, T. H. 1981 Trailing edge noise prediction using measured surface pressures. *J. Sound Vibr.* 78, 69-117.
- CHASE, D. M. 1980 Modeling the wave-vector frequency spectrum of turbulent boundary layer wall pressure. *J. Sound Vibr.* 70, 29-68.
- CORCOS, G. M. 1963 On the resolution of pressure in turbulence. . *J. Acoust. Soc. Am.* 35, 192-199.
- GERSHFELD, J. L., BLAKE, W. K. AND KNISLEY, C. K. 1988 Trailing edge flows and aerodynamic sound. AIAA-88-3826-CP *First National Fluid Dynamics Congress*, 2133-2140.
- HOWE, M. S. 1978 A review of the theory of trailing edge noise. *J. Sound Vibr.* 61, 473-465.
- HOWE, M. S. 1979 The influence of surface rounding on trailing edge noise. *J. Sound Vibr.* 126(3), 503-523.
- HUNT, J. C., MOIN, P., MOSER, R. D. AND SPALART, P. R. 1987 Self similarity of two point correlations in wall bounded turbulent flows. *Proceedings of the 1987 Summer Program*, Center for Turbulence Research, NASA Ames/Stanford Univ., 25-36.
- KIM, J. 1989 On the structure of pressure fluctuations in turbulent channel flow. *J. Fluid Mech.* 205, 421-451.
- LILLEY, G. M. 1960 Pressure fluctuations in an incompressible turbulent boundary layer. *College of Aeronautics, Cranfield, Report No. 133*.
- NA, Y. AND MOIN, P. 1996 Direct numerical simulation of turbulent boundary layers with adverse pressure gradient and separation. Report No. TF-68, Thermosciences Division, Dept. of Mech. Eng., Stanford Univ.
- SCHLOEMER, H. H. 1967 Effects of pressure gradients on turbulent boundary wall pressure fluctuations. *J. Acoust. Soc. Am.* 42, 93-113.